Journal of Materials Science: Materials in Electronics (2018) 29:15502–15511
https://doi.org/10.1007/s10854-018-9105-1

White and yellow light emission from ZrO_2:Dy^{3+} nanocrystals synthesized by a facile chemical technique

A. Báez-Rodríguez[1] · D. Albarrán-Arreguín[2] · A. C. García-Velasco[1] · O. Álvarez-Fregoso[2] · M. García-Hipólito[2] · M. A. Álvarez-Pérez[3] · L. Zamora-Peredo[1] · C. Falcony[4]

Received: 20 November 2017 / Accepted: 12 April 2018 / Published online: 16 April 2018

Abstract
White and yellow light were obtained from ZrO_2:Dy^{3+} nanocrystals which were synthesized by the solvent evaporation technique. The crystalline structure was studied by X-ray diffraction, resulting in a tetragonal and monoclinic mixture phases of ZrO_2 when the powders were annealed at 600 °C and the zirconia monoclinic phase when they were thermal treated at 1000 °C. By means of atomic force microscopy images was observed that the synthesized powders are constituted by nanocrystals about 20 nm for the samples annealed at 600 °C, whereas samples annealed at 1000 °C were constituted by crystals about 135 nm, these features were confirmed by TEM images. Luminescence properties were analyzed by means of photo and cathodoluminescence; exhibiting emissions in the white light region of the chromatic diagram. In the case of photoluminescence white-warm color (x = 0.35, y = 0.37) was observed, which is close to pure white color; while for cathodoluminescence the emission was yellowish with coordinates (x = 0.39, y = 0.39) in the chromatic diagram. PL decay time measurements were carried out; a lifetime of 0.66 ms was found. In addition, the PL quantum efficiency was measured; the obtained value was as high as 45%.

1 Introduction

In the last decades, research on the optical properties of materials has intensified from the incorporation of rare earth ions, due to their high efficiencies and various applications, such as displays, screens activated by cathode ray tube, lighting panels, thermoluminescent dosimeters, X-ray intensifying screens, lighting lamps and, in general, in electroluminescent devices [1]. In this type of applications, it is necessary to acquire quality powders and films that emit in the three basic colors: blue, green and red [2]. In particular, there is a great interest in the development of multicolored and white light electroluminescent devices with which any other color can be obtained using suitable filters [3]. The luminescence from the trivalent dysprosium ion (Dy^{3+}) mainly consists of lines in the blue (470–550 nm, $^4F_{9/2} - {}^6H_{15/2}$) and yellow (570–600 nm, $^4F_{9/2} - {}^6H_{13/2}$) regions [4]. Dysprosium can be able to give rise, under certain conditions, to the emission of white light by the combination of its two main emissions [5].This is important, since most current solid state lighting devices use a combination of emissions from different sources (blue or ultraviolet excitation source with mixes phosphors) or from different rare earth ions, which combine their emissions to produce white light [2, 3]. So the main advantage of the dysprosium ion is that white light can be obtained with the use of only one impurity. The use of a suitable host lattice to incorporate rare earths also remains a subject of study, until now have been used crystalline and non-crystalline host lattices, such as: glasses [6–8], polycrystalline metal oxides [9, 10], organometallic compounds [11, 12] and a wide variety of semiconductor materials [13, 14]. Among

✉ A. Báez-Rodríguez
adibr_1@hotmail.com

1 Centro de investigación en Micro y Nanotecnología, Universidad Veracruzana, Calzada Ruiz Cortines 455, 94294 Boca del Río, Veracruz, Mexico

2 Departamento de Materiales Metálicos y Cerámicos, Instituto de Investigaciones en Materiales, Universidad Nacional Autónoma de México, A.P. 70-360, Coyoacán, 04510 Mexico City, D.F., Mexico

3 Laboratorio de Bioingeniería de Tejidos, Facultad de Odontología, Universidad Nacional Autónoma de México, Coyoacán, 04510 Mexico City, D.F., Mexico

4 Departamento de Física, Centro de Investigación y de Estudios Avanzados del Instituto Politécnico Nacional, Apdo. Postal 14-470, Delegación Gustavo A. Madero, CP. 07000 Mexico City, D.F., Mexico

the ceramic materials, zirconium oxide (ZrO_2, zirconia) is a material with high potential due to its remarkable properties, such as: low phonon energy when it is doped by rare earths [15], high transparency in the visible region of the spectrum electromagnetic, high chemical stability, high thermal expansion coefficient, low thermal conductivity, wide energy gap, etc. [16]. There is an extensive study of the mechanical and optical properties of zirconia, but in recent years, the interest in the study of luminescent properties it has increased, for example: ZrO_2:Eu^{3+} [17], ZrO_2:Tb^{3+} [18], ZrO_2:Mn^{3+} [19], showing that it is a good host lattice for rare earth and transition metals ions. Likewise, there are scarce works about ZrO_2:Dy^{3+} monoclinic phase nanocrystals, this phosphor has been already studied in film form [20, 21] and white light has been obtained with the combinations of the blue and yellow emissions from dysprosium ions. Many attempts have been made to obtain white light emission from the incorporation of activators (mainly rare earth ions) that produce blue, green and red light. Some problems have arisen, in these cases, mainly due to energy transfers between these activators which do not allow obtaining the pure white color. Additionally, it has been reported that the nanometric size of the constituent crystals of a material, among other effects, has a positive influence on the PL efficiency [22, 23]. The objective of the present investigation is fundamentally the study of phosphors (ZrO_2:Dy^{3+}) that produce white light with the incorporation of a single ion as activator of the luminescence (in this case the trivalent dysprosium). In addition, are studied the structural, morphological, photo (PL) and cathodoluminescent (CL) properties of ZrO_2:Dy^{3+} powders synthesized by the simple and not expensive solvent evaporation technique and annealed at different temperatures (600–1000 °C). The quantum efficiency (QE) was also measured.

2 Experimental details

ZrO_2:Dy^{3+} powders were synthesized by the solvent evaporation process. In this technique, the precursors are dissolved or mixed in some liquid solvent (water, alcohol, etc.) and kept in agitation for a few minutes, then the solvents are evaporated—generally by thermal means—and the powder thus obtained is annealed at different temperatures to complete its synthesis. The precursor materials used in this case were: zirconium oxychloride octahydrate ($ZrOCl_2{\cdot}8H_2O$, 99.9% purity, FLUKA) with a concentration of 0.05 M and dysprosium chloride hexahydrate ($DyCl_3{\cdot}6H_2O$, with a purity of 99.9%, ALFA-AESAR) in atomic percentages (at.%) of 0, 0.5, 2, 5 and 10, with respect to the Zr content in the mixture or solution; as a solvent, ethyl alcohol was used. In a typical case, 1.6 g of $ZrOCl_2{\cdot}8H_2O$ are mixed in 100 milliliters of ethyl alcohol. This mixture was kept in constant agitation for 10 min to achieve a better distribution of the precursors, later it was dried at a temperature of 250 °C for 15 min, until obtaining a yellow-orange powder. The powders thus obtained were annealed (in alumina crucibles) at five different temperatures: 600, 700, 800, 900 and 1000 °C during 4 h in an air atmosphere. Finally, these white powders were ground in an agate mortar. For the characterizations, samples were prepared as cylindrical tablets of 12 mm in diameter and 3 mm in thickness (compressing the powders in a press with a pressure of 5 tons for 10 min). The crystalline structure of the synthesized materials was determined by means of X-ray diffraction (XRD) using a Siemens D-5000 diffractometer that uses typical copper target radiation ($k\alpha = 1.5406$ Å). The elemental chemical composition was measured by means of energy dispersive spectroscopy (EDS) with a scanning electron microscope (SEM) JEOL, model JSM-7600F equipped with an X-ray detector Oxford INCA Energy +, Si–Li. The surface morphology of the powders was observed by SEM with the aforementioned microscope. The average crystal size and some features of the surface morphology were also appreciated using a JEOL model JCPM-4210 atomic force microscope (AFM). TEM images were acquired by means of a transmission microscope JEOL model JEM-ARM 200F. The photoluminescent properties of the powders were recorded using a Fluoro-Max-P spectrofluorimeter from Jobin Yvon Horiba. The PL decay time measurements were recorded with an Edinburgh Instruments fluorescence spectrometer model FLS980 equipped with an integration sphere to quantum efficiency (QE) measurements. The cathodoluminescence of these materials was measured by placing the sample in a vacuum chamber of stainless steel with a cold cathode electron gun (Luminoscope model ELM-2 MCA, RELION Co.). The pressure of said chamber is $< 10^{-3}$ Torr. The beam of electrons used to excite the samples is parallel to the surfaces of the same, by means of a magnetic field; this one is deviated 90° to descend perpendicular to the samples surface. The visible radiation emitted by the analyzed powders is transported by an optical fiber to the aforementioned spectrofluorimeter, where it is analyzed. Variations were made in the value of the accelerating voltage of the incident electrons; the current of the electron beam was set at 0.3 mA and the beam diameter was 0.5 cm.

3 Results and discussion

Figure 1 shows the diffractograms for the ZrO_2:Dy^{3+} (0.5 at.%) powders as a function of the annealing temperature. The annealing temperatures were varied from 600, 700, 800, 900 up to 1000 °C. Tetragonal phase at 600 °C (01-079-1764, ICSD 066783) and monoclinic phase (JCPDS 37-1484) at 1000 °C were indexed. The actual percentages

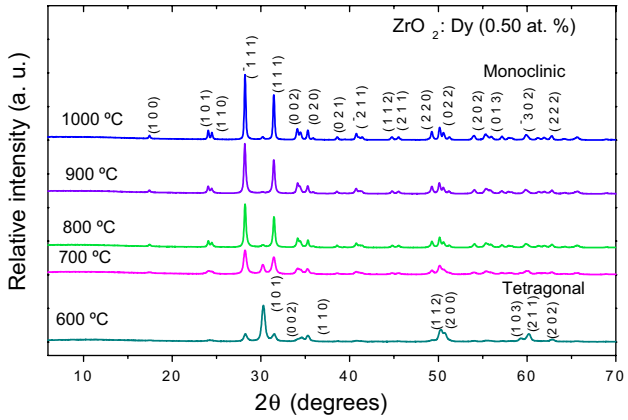

Fig. 1 X-ray diffractograms of ZrO_2:Dy^{3+} (0.50 at.%) nanocrystals, for different annealing temperatures (600–1000 °C)

of the phases were calculated using the database ICCD-PDF-02, diffract plus of Bruker ASX, EVA software, which are tabulated in Table 1. At low temperatures there is the presence of a mixture of the tetragonal and monoclinic phases of zirconia, almost in a 1:1 ratio. The sample annealed at 700 °C showed the presence of monoclinic phase almost entirely, with 90.66%, which indicates that at this temperature the transformation of tetragonal to monoclinic phase had already been carried out completely. In addition, it is noted that as the annealing temperature increased the percentage of monoclinic phase increases up to 99.55% for the thermally treated samples at 1000 °C, which can be explained because at low temperature the formation of the tetragonal phase is favored [24, 25]. Moreover, an increase in the crystal size was observed as the temperature was higher, especially for the monoclinic phase ($\bar{1}11$), since for the tetragonal phase (101) it was imperceptible for samples annealed at 900 and 1000 °C (see Table 1). These values are close to those observed in the images obtained by AFM. The values of the full width at half maximum (FWHM) of the plane ($\bar{1}11$) is a measure of the perfection of the crystalline structure. The decrease in the values of the FWHM, indicate an increase in the crystalline quality of the samples as a function of the growth in the annealing temperature. The changes in FWHM and crystal size are good proof of the successful doping of Dy^{3+} ions in ZrO_2, moreover, the results of EDS are in concordance with these parameters, since at high doping content the crystal size decreases, similar doping studies have been carried out in other investigations [26, 27].

Table 2 shows the elemental composition of the ZrO_2:Dy^{3+} powders annealed at 1000 °C with variations of the $DyCl_3$ concentrations in the precursor mixture (0, 0.25, 0.50, 2, 5 and 10 at.%, in relation to the content of Zr). It is noted that as $DyCl_3$ is added the atomic percentage of Dy^{3+} and Cl increase, and the atomic percentages of Zr and O decrease slightly. This could indicate that the host lattice (ZrO_2) is suitable for the incorporation of the luminescence activator centers (Dy^{3+} ions). Table 3 shows the atomic percentages of Zr, O, Dy and Cl, present in the powders of ZrO_2:Dy^{3+} (0.50 at.%) considering variations in the value

Table 1 Percentage of the crystalline phase, FWHM and crystallite size of ZrO_2:Dy^{3+} (0.50 at.%) nanocrystals, for different annealing temperatures

Cristal phase			Tetragonal		Monoclinic	
Sample (°C)	Tetragonal %	Monoclinic %	Crystal size (nm)	FWHM (radians)	Crystal size (nm)	FWHM (radians)
600	56.11	43.89	21.92	0.417	24.60	0.370
700	9.34	90.66	27.47	0.333	34.93	0.365
800	1.40	98.60	31.14	0.294	37.22	0.245
900	0.81	99.19	–	–	59.27	0.232
1000	0.45	99.55	–	–	87.46	0.192

Table 2 Atomic percent content of the oxygen, zirconium, dysprosium and chlorine, present in nano-powders of ZrO_2:Dy^{3+} as measured by EDS, synthesized with different concentrations of $DyCl_3$ in the initial mixture

$DyCl_3$ (at.%)	Oxygen (at.%)	Zirconium (at.%)	Dysprosium (at.%)	Chlorine (at.%)
0	66.87	32.64	0	0.49
0.25	66.58	32.78	0.12	0.52
0.5	66.46	32.48	0.26	0.80
2	65.69	32.43	0.43	1.45
5	64.47	32.63	0.99	1.91
10	63.65	31.57	2.29	2.49

The annealing temperature was 1000 °C

Table 3 Atomic percent content of the oxygen, zirconium, dysprosium and chlorine, present in nano-powders of ZrO_2:Dy^{3+} measured by EDS, annealed at different temperatures

T (°C)	Oxygen (at.%)	Zirconium (at.%)	Dysprosium (at.%)	Chlorine (at.%)
600	63.12	31.62	2.25	3.01
700	63.95	31.80	1.82	2.43
800	64.59	31.01	1.57	1.83
900	65.87	32.18	0.73	1.22
1000	66.46	32.48	0.26	0.80

The content of $DyCl_3$ remained constant at 0.5 at.%

of the annealing temperature. Here it is possible to observe that as the annealing temperature increases the values of Zr and O increase a little bit and those of Dy and Cl decrease. In all cases it can be seen that the ratio Zr/O is close to the ideal (0.5).

SEM micrographs of ZrO_2:Dy^{3+} (0.5 at.%) powders annealed at 600 and 1000 °C are shown in Fig. 2. Images with an amplification of 50 kX are showed in Fig. 2a, b. Figure 2a shows the sample annealed at 600 °C where it is possible to notice rough surfaces constituted by agglomerates of irregular particles. Here particles > 100 nm are observed. In addition, some pores are detected, which are produced by the exit of the residual gases of the chemical reaction (chlorine, water vapor and combinations of them). Figure 2b exhibits the morphological features of the sample annealed at 1000 °C, in this case larger particles are observed, some of them seem to have well-defined geometrical forms; this effect is probably due to the higher annealing temperature. SEM images were also obtained for samples with different amounts of the doping concentration but no one notable changes were observed in their morphology.

AFM images for ZrO_2:Dy^{3+} (0.5 at.%) powders are presented in Fig. 3. The Fig. 3a shows an image of the sample annealed at 600 °C, it is possible to see crystals or grains in elongated shape and of very different sizes, on average the size was about 20 nm. Figure 3b shows an image of an annealed sample at 1000 °C, here it is possible to observe grains with a more spherical or rounded geometry and larger sizes; in this case the average crystal size was about 135 nm. This growth in the crystal size is probably due to the increase in the annealing temperature; in this case the higher available thermal energy leads to a re-crystallization

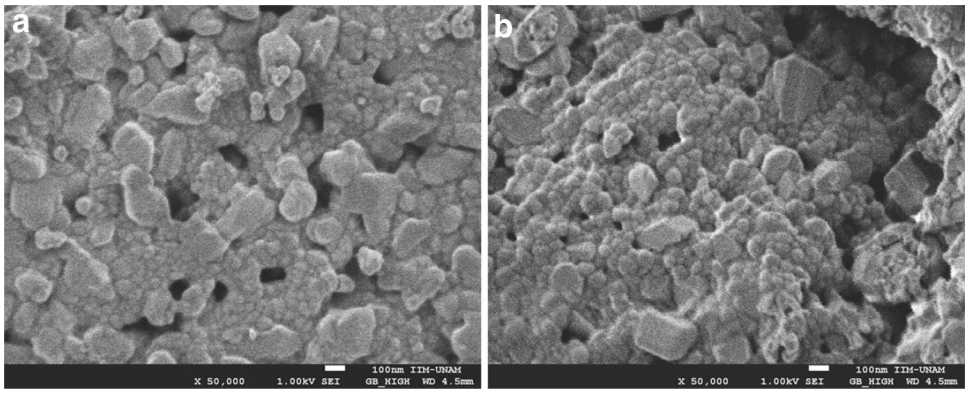

Fig. 2 SEM micrographs for ZrO_2:Dy^{3+} (0.50 at.%) nanocrystals annealed at **a** 1000 °C and **b** 600 °C

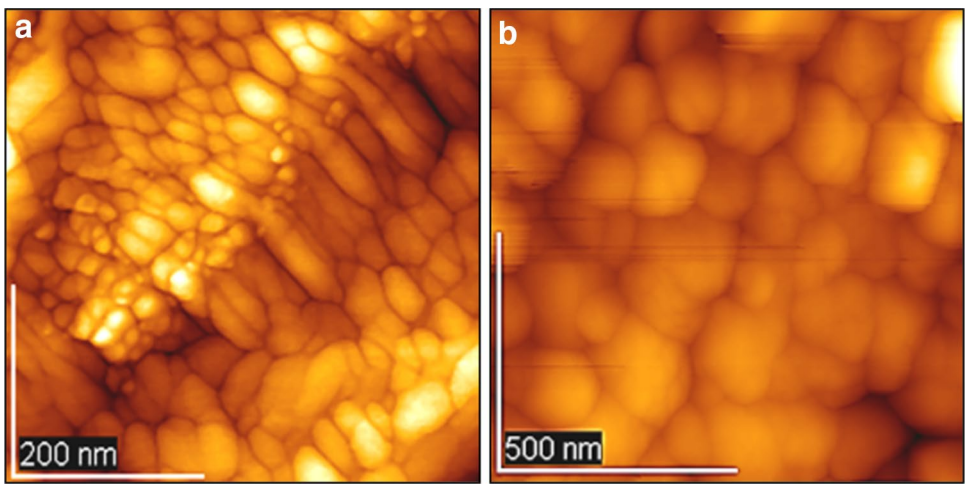

Fig. 3 AFM images for ZrO_2:Dy^{3+} (0.50 at.%) nanocrystals annealed at **a** 600 °C and **b** 1000 °C

which propitiates the growth of some crystals at the expense of many others.

Figure 4 illustrates the TEM micrographs for nanocrystalline ZrO_2:Dy^{3+} (0.5 at.%) powders annealed at 600 and 1000 °C. Figure 4a, b correspond to samples annealed at 1000 °C; as can be seen from the images, these samples consist of particles ranging in size < 200 nm and have irregular shapes; it is also possible to observe irregularly shaped crystals > 50 nm (Fig. 4b). Figure 4c, d show TEM images for the sample annealed at 600 °C; in this case, rounded particle clusters of approximately 20–30 nm are observed (Fig. 4c), it is also possible to appreciate crystals whose size is approximately 10–20 nm (Fig. 4d). Here it is concluded that the effect of the annealing temperature is to produce an increase in the size of the crystals as that temperature increases. These results verify that the size of the crystals is a few tens of nanometers and also confirms the results obtained by AFM and XRD analysis.

Figure 5 displays the PL excitation spectrum for ZrO_2:Dy^{3+} (0.5 at.%) powders annealed at 1000 °C. The emission wavelength was fixed at 580 nm, corresponding to the band with yellow emission of the Dy^{3+} ions. The highest intensity of excitation is reached in a broad band of 200–250 nm, centered at 238 nm, which is attributed to the absorption of the host lattice ZrO_2 [28]. Simultaneously, although with less intensity, characteristic absorptions

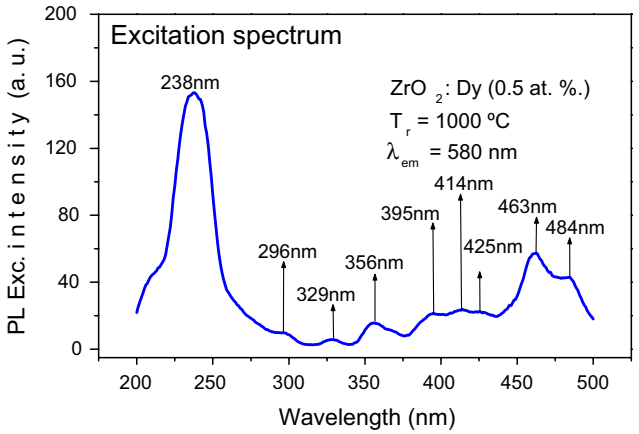

Fig. 5 PL excitation spectrum for ZrO_2:Dy^{3+} (0.50 at.%) nanocrystals annealed at 1000 °C

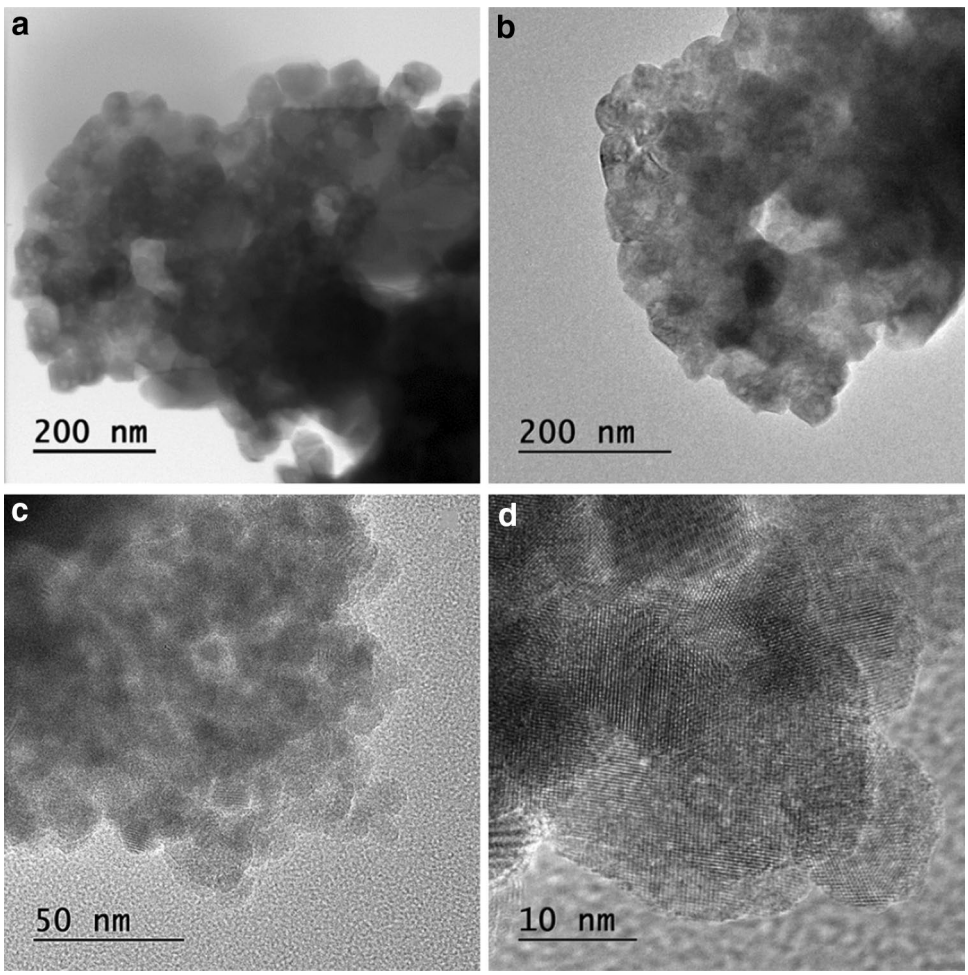

Fig. 4 TEM micrographs for ZrO_2:Dy^{3+} (0.50 at.%) nanocrystals annealed at **a, b** 1000 °C and **c, d** 600 °C

of the Dy^{3+} ions are observed, located at 296, 329, 256, 395, 414, 425, 463, and 484 nm, which correspond to the absorptions from base state $^6H_{15/2}$ to excited states: $^4D_{7/2}$ (296 nm),$^6P_{3/2}$ (329 nm), $^6P_{7/2}$ (356 nm),$^4F_{7/2}$ (385 nm), $^4M_{21/2}+^4I_{13/2}+^4K_{17/2}+^4F_{7/2}$ (from 375 to 414 nm), $^4G_{11/2}$ (463 nm), $^4F_{9/2}$ (484 nm) [29–31]. From this spectrum, a radiation with a wavelength of 238 nm is selected to excite the materials studied in this work.

Figure 6 shows the PL emission spectra for ZrO_2:Dy^{3+} powders with variations in the content of Dy^{3+} ions (0, 0.25, 0.5, 2, 5, 10 at.%) in the precursor mixtures; these samples were annealed at 1000 °C and are excited with a wavelength of 238 nm. In this case, several features can be distinguished: the spectra labeled with the letters a–e present the characteristic emissions of the Dy^{3+} ion: $^4F_{9/2}\rightarrow{}^6H_{15/2}$, $^4F_{9/2}\rightarrow{}^6H_{13/2}$, $^4F_{9/2}\rightarrow{}^6H_{11/2}$, and $^4F_{9/2}\rightarrow{}^6H_{9/2}$, centered at 490, 580, 674 and 761 nm, respectively. It should be noted that the two most intense emissions, the blue centered at 490 nm and the yellow centered at 580 nm, are almost of the same intensity, there is a good balance between the yellow band, electronic dipole transition, and blue band attributed to magnetic dipole transition, this behavior allows an optimal combination of these emissions to obtain white light emission [32]. As expected, it is also observed all powders with any content of Dy^{3+} ions have higher emission intensity than that sample without Dy^{3+} ions (Fig. 5f); as the content of Dy^{3+} ions increases, the emission intensity intensifies, reaching its maximum at 0.5 at.% of Dy^{3+} ions, after this amount the concentration quenching is reached, causing a decrease in the emission intensity as the content of Dy^{3+} ions increases for 2, 5 and 10 at.%, this is explained by the fact that due to the high concentration of Dy^{3+} ions, they are so close to each other that a transfer of the excitation energy takes place from one to another until that this energy is lost in an energy sink.

Figure 7 exhibits the PL emission spectra for ZrO_2:Dy^{3+} (0.5 at.%) powders with variations in the annealing temperature (600, 700, 800, 900 and 1000 °C), the excitation wavelength again was 238 nm. These spectra also present the two most intense bands, blue and yellow, centered at 490 nm ($^4F_{9/2}\rightarrow{}^6H_{15/2}$) and 580 nm ($^4F_{9/2}\rightarrow{}^6H_{13/2}$), the weakest are centered at 674 and 761 nm, which correspond to the electronic transitions $^4F_{9/2}\rightarrow{}^6H_{11/2}$, and $^4F_{9/2}\rightarrow{}^6H_{9/2}$, respectively. It is noted that the emission intensity increases as the annealing temperature does; the sample processed at the highest temperature (1000 °C) has the maximum intensity of PL emission, which can be explained taking into account the results of XRD obtained, in which the crystallinity of the powders increases as a function of the increase in the annealing temperature, that is, a better crystalline arrangement of the material and the reduction of unwanted impurities contributes to a more uniform distribution of the luminescent centers (Dy^{3+}), which guarantees the absence of inhibitions of luminescence due to the closeness between the doping ions when they are not properly distributed. Additionally, the purity of monoclinic phase was improved with the increase of annealing temperature, and this could contribute to a better arrangement of Dy^{3+} ions.

The spectra for CL emission for ZrO_2:Dy^{3+} (0.5 at.%) powders, as a function of the electron accelerating voltage (4, 6, 8, 12 and 14 kV) can be seen in Fig. 8; the annealing temperature of these samples was 1000 °C. It is observed that as the electron acceleration voltage increases, the intensity of the CL also grows, the excitation with 14 kV generates the highest emission intensity; This is due to the

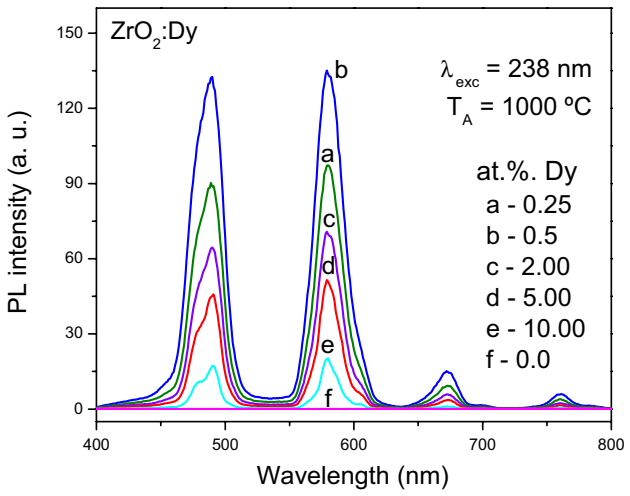

Fig. 6 PL emission spectra for ZrO_2:Dy^{3+} (0.50 at.%) nanocrystals annealed at 1000 °C, as a function of the doping concentration; the excitation wavelength was 238 nm

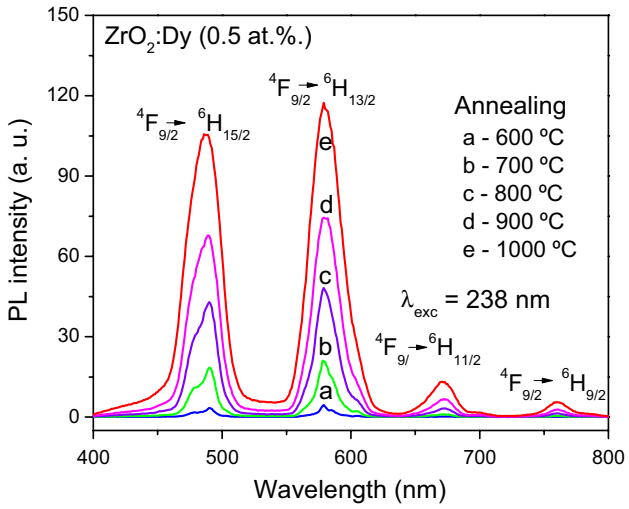

Fig. 7 PL emission spectra for ZrO_2:Dy^{3+} (0.50 at.%) nanocrystals as a function of the annealing temperature (600, 700, 800, 900 and 1000 °C); the excitation wavelength was 238 nm

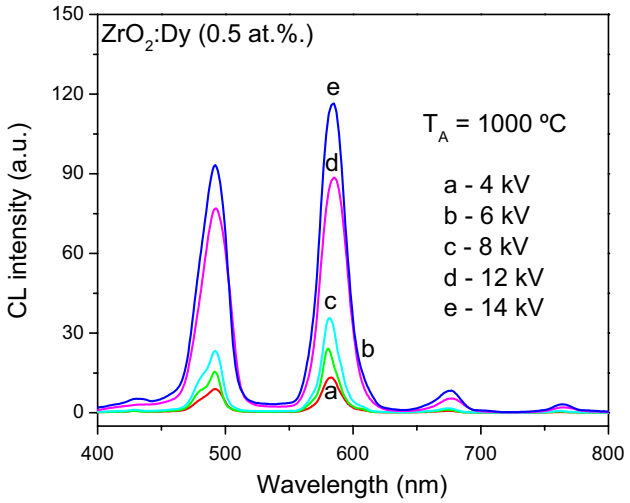

Fig. 8 CL emission spectra for ZrO_2:Dy^{3+} (0.50 at.%) nanocrystals annealed at 1000 °C, as a function of the electron accelerating voltage

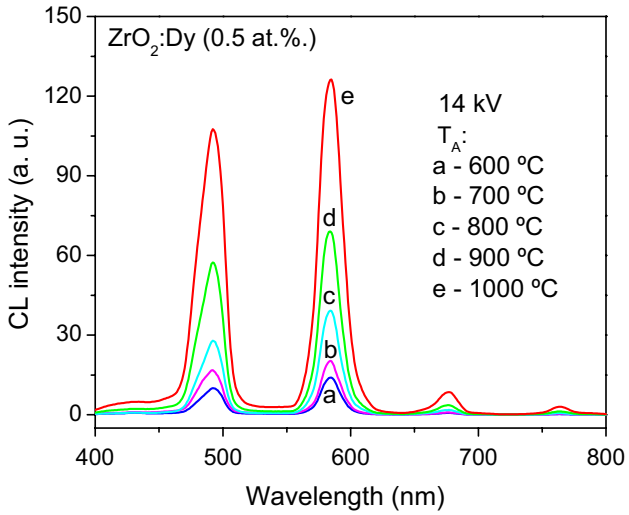

Fig. 9 CL emission spectra for ZrO_2:Dy^{3+} (0.50 at.%) nanocrystals annealed, as a function of the annealing temperatures (600, 700, 800, 900 and 1000 °C). The electron accelerating voltage was 14 kV

fact that at higher electron acceleration voltages the penetration of the incident electrons is greater inside the sample, which produces the excitation of a greater volume and therefore a greater number of luminescent centers, which contribute to a greater intensity of the CL emission. The characteristic emissions of the Dy^{3+} ion, $^4F_{9/2} \rightarrow {}^6H_{15/2}$ (490 nm), $^4F_{9/2} \rightarrow {}^6H_{13/2}$ (580 nm), $^4F_{9/2} \rightarrow {}^6H_{11/2}$ (674 nm) are observed, as in photoluminescence, and $^4F_{9/2} \rightarrow {}^6H_{9/2}$ (765 nm). Similar to the photoluminescence spectra, the most intense bands are blue and yellow; in this case (CL), it is observed that the blue band is less intense than the yellow band. This change can be attributed to the fact that the excitation of the material is of a different nature, as the accelerated electrons are much more energetic than photons. This difference in energies produces other phenomena as a result of the interaction of accelerated electrons with matter. Among other phenomena, secondary electrons, Auger electrons, retro-scattered electrons, X-rays, etc. are produced, which can also excite the doping ions and can even produce changes in the environment of the Dy^{3+} ions [33]. In this way, the difference in the spectra of photo and cathodoluminescence, could be due mainly to the fact that the yellow band of ZrO_2:Dy^{3+} powders is of an electrical nature, that is, it depends on the crystalline field generated by its environment while the blue band, which is magnetic in nature, is not as influenced by the surroundings of the doping ion. These facts explain why the CL emissions are more yellowish than that obtained for the PL.

In Fig. 9, the spectra of CL are shown for ZrO_2:Dy^{3+} (0.5 at.% the initial mixture) powders considering changes in the annealing temperature (600, 700, 800, 900 and 1000 °C). The electron accelerating voltage was 14 kV. In this case, the characteristic transitions of the Dy^{3+} ion are again observed, and like Fig. 7, the most intense band is centered at 580 nm (yellow band). The behavior of the CL emission intensity as a function of the annealing temperature is similar to that for PL, that is, in the spectra it is clearly seen that the emission intensity increases as the annealing temperature does. As in the case of the PL, this behavior is attributed to the fact that at higher temperatures, the available thermal energy helps to eliminate a greater amount of defects such as the remaining impurities (chlorine, water vapor), as well as producing a more crystalline material, in which the luminescent centers can have a better distribution where energy transfers are minimized, which contributes to a greater number of them generating photons and with this a greater intensity of the emitted light.

Figure 10 displays the CL spectra for ZrO_2:Dy^{3+} powders with variations in dopant concentration, Dy^{3+} (0, 0.25, 0.50, 2, 5, and 10 at.%). The accelerating voltage of the exciting electrons was 14 kV. For these samples the annealing temperature was 1000 °C. As in all the previous spectra (Figs. 5, 6, 7, 8), the characteristic emissions of the Dy^{3+} ion are observed. The band in the yellow region, centered at 580 nm, is the most intense again. The increase in CL intensity is favored by increasing the content of Dy^{3+} ions up to a certain value. The highest intensity of the emission is achieved for a concentration of 0.5 at.% of Dy^{3+} ions, after which, the intensity CL decays progressively for contents of 2, 5 and 10 at.%, the above is attributed, as in the case of PL, to a luminescence inhibition due to high doping concentration.

In Fig. 11, the Commission Internationale de l'Éclairage (CIE) chromaticity diagram is observed for the PL and CL from ZrO_2:Dy^{3+} (0.5 at.%) powders annealed at 1000 °C. It can be noticed that the powders present a white-warm

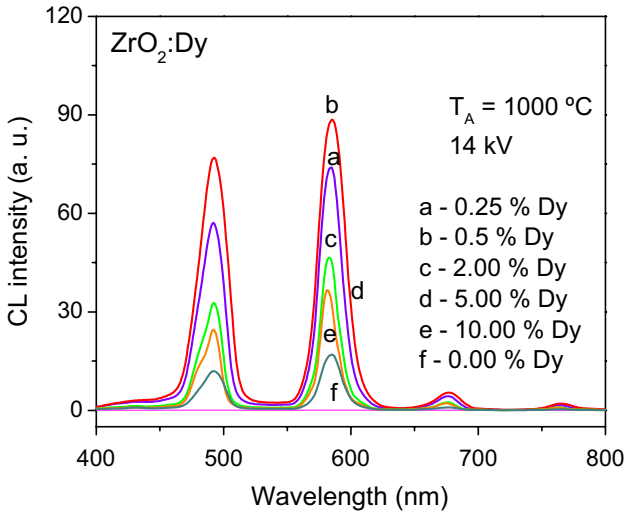

Fig. 10 CL emission spectra for ZrO_2:Dy^{3+} (0.50 at.%) nanocrystals annealed at 1000 °C, as a function of the doping concentration. The electron accelerating voltage was 14 kV

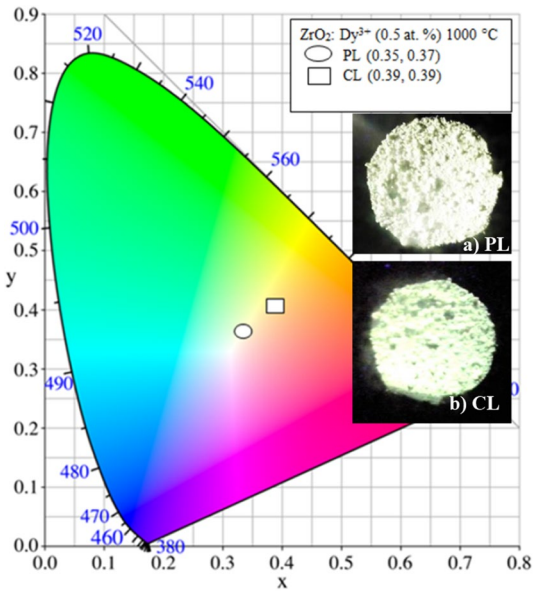

Fig. 11 CIE chromaticity diagram for the PL and CL of ZrO_2:Dy^{3+} (0.5 at.%) nanocrystals annealed at 1000 °C. Insets show their snapshot for: **a** PL; excited by a UV lamp (4 W) with 254 nm and **b** CL; excited by accelerated electrons, 14 kV

emission (white-yellow), with coordinates (0.35, 0.37) for the PL emission which is very close to the pure white (0.33, 0.33) and a yellowish color for the CL emissions (0.39, 0.39). The difference in the color emission between PL and CL is due to the fact that, as mentioned above, in CL the most intense band was the yellow band of the Dy^{3+} ions centered at 580 nm, which contributes even more to the emission shifting to the yellowish region of the chromatic diagram. Digital photographs for ZrO_2:Dy^{3+} (0.5 at.%) samples, annealed at 1000 °C, are shown in inset of Fig. 11a, b. These powders were excited by an UV-lamp (254 nm), inset (a) and an electron beam of 14 kV, inset (b). It can be observed a light yellowish color for CL and a warm white color for PL. Although there are no photographs of these samples excited by 238 nm (PL optimal excitation), they are expected to be even more intense than that shown.

Life-time measurements for ZrO_2:Dy^{3+} (0.5 at.%) were performed by excitation with 238 nm monitoring the emissions at 490 nm (blue) and 580 nm (yellow); Fig. 12a, b shows the decay profiles associated with Dy^{3+} ions. The decay curves for transitions of Dy^{3+} ions were fitted with a double-exponential function: $I(t) = A + B_1\exp(-t/\tau_1) + B_2\exp(-t/\tau_2)$, where $I(t)$ represents the PL intensity and A (background), B_1, B_2, and τ_1, τ_2 designate the fitting parameters. The bi-exponential decay suggests the possibility that Dy^{3+} ions are placed in two different sites or this behavior is due to effects generated by the energy transfer or even to certain defects of the host lattice [34, 35]. However, more studies are underway to fully elucidate this fact. The average decay times, τ_{av}, were calculated with fitting parameters and the following equation: $\tau_{av} = [\Sigma B_i(\tau_i)^2]/[\Sigma B_i(\tau_i)]$. The average decay times calculated from these fits were 0.66 and 0.61 ms, which are very similar to that reported in other investigations [35, 36].

The PL quantum efficiency (QE) is one of the most important characteristics in the application of luminescent materials. This QE was measured several times in ZrO_2:Dy^{3+} (0.5 at.%) samples, the averaged value obtained was 45%, when it was excited with 238 nm. The QE values were computed by the following equation [37]:

$$\eta(QE) = \frac{\int L_{emission}}{\int E_{blanc} - \int E_{sample}}$$

where $L_{emission}$ is the emission spectrum of the studied film, E_{sample} is the spectrum of the light used for exciting the film and E_{blanc} is the spectrum of the excitation light without the sample in the integration sphere. The calculated QE values for ZrO_2:Dy^{3+} (0.5 at.%) powders is remarkable and as high as that of other materials that already have a practical application [38].

4 Conclusions

ZrO_2:Dy^{3+} luminescent nanocrystals were obtained successfully by means of the solvent evaporation technique which is very simple and relatively inexpensive; capable of producing good quality powders with the appropriate requirements for application as luminescent materials in the warm-white region of the chromatic diagram. X-ray

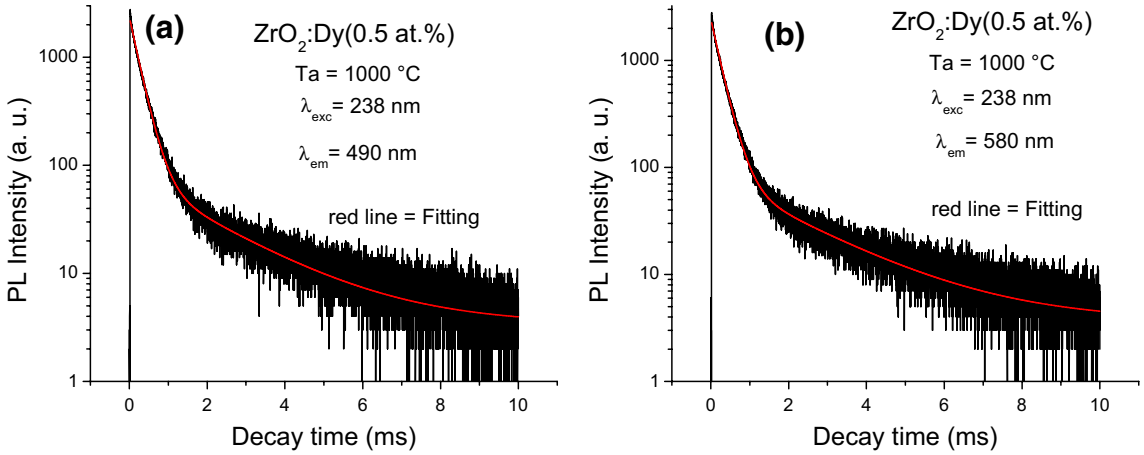

Fig. 12 PL decay time curves for ZrO_2:Dy^{3+} (0.5 at.%) annealed at 1000 °C, by excitation with 238 nm monitoring the emissions at **a** 490 nm (blue) and **b** 580 nm (yellow)

diffraction analysis showed that the crystalline quality of the ZrO_2:Dy^{3+} powders depended on the annealing temperatures; at the lowest temperature (600 °C) the crystalline structure was a mixture of tetragonal and monoclinic ZrO_2 phases whereas for the higher temperature, 1000 °C, the phase was the monoclinic of ZrO_2. SEM micrographs show rough surfaces formed by irregularly shaped particle clusters with some pores. AFM images exhibit surfaces constituted by irregularly shaped particles of some tens of nanometers and the TEM images show crystals whose size coincides reasonably with those shown in AFM and XRD analysis. PL and CL emission spectra exhibited the characteristic emissions of the Dy^{3+} ions and the highest intensity was reached with 0.5 at.% of Dy^{3+} ions (in the precursor mixture) and the optimal annealing temperature was 1000 °C. In PL spectra, the most intense bands were the blue at 490 nm and the yellow one at 580 nm, which have almost the same intensity, whereas in CL spectra the yellow band was more intense followed by the blue band. Due to the similarity in intensities of the two main bands of Dy^{3+} ions in PL, the chromatic diagram assigns coordinates (0.35, 0.37), which correspond to a white-warm color, very close to pure white. ZrO_2:Dy^{3+} nanocrystals display strong emissions in the white and yellow colors visible to naked eyes with a quantum efficiency of 45%, which is remarkable. Also the cathodoluminescence studies are very scarce or nonexistent in this material. The average PL decay times for ZrO_2:Dy^{3+} (0.5 at.%) were 0.66 and 0.61 ms, which are very similar to that reported in other investigations for Dy^{3+} ions. Finally, it is convenient to emphasize the importance of obtaining the emission of white light from ZrO_2 nano-powders activated with a single activator (Dy^{3+}), without the need to incorporate other impurities, which is not always possible.

Acknowledgements The authors thank to Adriana Tejeda for the XRD measurements and to Daniel de Jesús Araujo Perez for their for the XRD analysis, to Omar Novelo for the SEM micrographs, to Josué Romero for TEM images, Carlos Flores for the AFM images and to Marcela Guerrero, Zacarías Rivera, Raúl Reyes and Alberto López for their technical support.

References

1. S. Lange, V. Kiisk, V. Reedo, M. Kirm, J. Aarik, I. Sildos, Opt. Mater. **28**, 1238–1242 (2006)
2. Z. Xie, Z. Yin, Y. Wu, C. Liu, X. Hao, Q. Du, X. Xu, Nat. Sci. Rep. **7**, 12146 (2017)
3. J. Cho, J.H. Park, J.K. Kim, E.F. Schubert, Laser Photonics Rev. **11**(2), 1600147 (2017)
4. M.M. Kimani, J.W. Kolis, J. Lumin. **145**, 492–497 (2014)
5. S. Chemingui, M. Ferhi, K. Horchani-Naifer, M. Férid, J. Lumin. **166**, 82–87 (2015)
6. Y.C. Ratnakaram, D.T. Naidu, A. Vijayakumar, J.L. Rao, Opt. Mater. **27**, 409–417 (2004)
7. S. Tanabe, J. Kang, T. Hanada, N. Soga, J. Non-Cryst. Solids **239**, 170–175 (1998)
8. P. Babu, C.K. Jayasankar, Opt. Mater. **15**, 65–79 (2000)
9. H.W. Zhang, X.Y. Fu, S.Y. Niu, C.G. Sun, Q. Xim, Solid State Commun. **132**, 527 (2004)
10. D. Van der Voort, G. Blasse, Chem. Mater. **3**, 1041–1045 (1991)
11. K. Hanaoka, K. Kikichi, H. Kojima, Y. Urano, T. Nagano, J. Am. Chem. Soc. **126**, 12470–12476 (2004)
12. Z. Hong, W.L. Li, D. Zhao, C. Liang, X. Liu, J. Peng, Synth. Met. **111**, 43 (2000)
13. I.T. Weber, A.P. Maciel, P.N. Lisboa-Filho, E. Longo, E.R. Leite, Nano Lett. **2**, 969–973 (2002)
14. H. Choi, C.H. Kim, C.H. Pyun, S.J. Kim, J. Lumin. **82**, 25–32 (1999)
15. C. Urlacher, J. Dumas, J. Serughetti, J. Mugnier, M. Muñoz, J. Sol-Gel. Sci. Technol. **8**, 999–1005 (1997)
16. A. Gendaken, R. Reisfeld, E. Sominsky, O. Palchik, Yu Kiltypin, G. Pancer, M. Gaft, H. Minti, J. Phys. Chem. B **204**, 7075 (2000)
17. H.W. Zhang, X.Y. Fu, S.Y. Niu, Q. Xin, Mater. Chem. Phys. **91**, 361–364 (2005)

18. J.C. Pivin, N.V. Gaponenco, I. Molchan, R. Kudrawiec, J. Misiewicz, J. Alloys Compd. **341**, 272–274 (2002)
19. M. Garcia-Hipolito, O. Alvarez-Fregoso, E. Martínez, C. Falcony, M.A. Aguilar-Frutis, Opt. Mater. **20**, 113–118 (2002)
20. A. Baéz-Rodríguez, O. Alvarez-Fragoso, M. García-Hipólito, J. Guzmán-Mendoza, C. Falcony, Ceram. Int. **41**, 7197–7206 (2015)
21. R.C. Martínez-Olmos, J. Guzmán-Mendoza, A. Báez-Rodríguez, O. Álvarez-Fragoso, M. García-Hipólito, C. Falcony, Opt. Mater. **46**, 168–174 (2015)
22. R.N. Bhargava, D. Gallagher, Phys. Rev. Lett. **72**, 416–419 (1994)
23. P. Haritha, C.S.D. Viswanath, K. Linganna, P. Babu, C.K. Jayasankar, V. Lavín, V. Venkatramu, J. Lumin. **179**, 533–538 (2016)
24. Y. Gao, Y. Masuda, H. Ohta, K. Koumoto, Chem. Mater. **16**, 2615–2622 (2004)
25. M.A. Waghmare, K.S. Pawar, H.M. Pathan, A.U. Ubale, Mater. Sci. Semicond. Process. **72**, 122–127 (2017)
26. J. Jalali, M. Mozammel, J. Mater. Sci.: Mater. Electron. **28**, 5336–5343 (2017)
27. J. Jalali, M. Mozammel, M. OjaghiIlkhchi, J. Mater. Sci.: Mater. Electron. **28**, 16776–16787 (2017)
28. P. Haritha, I.R. Martín, C.S.D. Viswanath, N. Vijaya, K.V. Krishnaiah, Opt. Mater. **70**, 16–24 (2017)
29. X. Fua, S. Niu, H. Zhang, Q. Xin, Mater. Sci. Eng. B **129**, 14–17 (2006)
30. Q. Du, G. Zhou, J. Zhou, X. Jia, H. Zhou, J. Alloys Compd. **552**, 152–156 (2013)
31. C.-H. Liang, L.-G. Teohb, K.T. Liu, Y.-S. Chang, J. Alloys Compd. **517**, 9–13 (2012)
32. Y. Shi, Y. Wang, Z. Yang, J. Alloys Compd. **509**, 3128–3131 (2011)
33. O. Lyuji, *Cathodoluminescence Theory and Applications* (Kodansha Ltd., Tokio, 1990), pp. 3–36
34. G. Jia, Y. Song, M. Yang, Y. Huang, L. Zhang, H. You, Opt. Mater. **31**, 1032–1037 (2009)
35. G. Phaomei, W. Singh, R.S. Ningthoujam, J. Lumin. **131**, 1164–1171 (2011)
36. I.A. Rayappan, K. Marimuthu, S.S. Babu, M. Sivaraman, J. Lumin. **130**, 2407–2412 (2010)
37. T. Li, P.L. Li, Z.J. Wang, S.C. Xu, Q.Y. Bai, Z.P. Yang, Dalton Trans. **44**, 16840–16846 (2015)
38. H. Deng, N. Xue, Z. Hei, M. He, T. Wang, N. Xie, R. Yu, Opt. Mater. Express **5**, 490–496 (2015)